Architecture characterization of orchard trees for mechanical behavior investigations

Min-Kyung Jeon
Matthew Burrall
Tae-Hyuk Kwon
Jason DeJong (jdejong@ucdavis.edu)
UC Davis: University of California Davis https://orcid.org/0000-0002-9809-955X
Alejandro Martinez

Research Article

Keywords: Root architecture, 3D root model, Skeleton, Statistical variation, Branching angle, Bifurcation, Mechanical pull-out

Posted Date: May 11th, 2022

DOI: https://doi.org/10.21203/rs.3.rs-1559682/v1

Abstract

Aims

This study explores structural root architectures of orchard trees to understand the interplays between the mechanical behavior of roots and the root architecture.

Methods

Full three-dimensional (3D) models of natural tree root systems, Lovell, Marianna, Myrobalan, that were extracted from the ground by vertical pullout are reconstructed through photogrammetry, and later skeletonized as nodes and root branch segments. Combined analyses of the full 3D models and skeletonized models enable detailed examination of basic bulk properties and quantification of architectural parameters. The segments from the skeletonized models are divided into three categories — trunk roots, main lateral roots, and remaining roots.

Results

The patterns in branching and diameter distributions show significant difference between the trunk and main laterals versus the remaining lateral roots. In general, the branching angle decreases over the course of successive bifurcations. The main lateral roots near the trunk show significant spreading while the lateral roots near the end tips grow roughly parallel to the parent root. For branch length, the roots bifurcate more frequently near the trunk than further from the trunk. The local thickness analysis confirms that the root diameter decays at a higher rate near the trunk than in the remaining lateral roots, while the total cross-sectional area across a bifurcation node remains mostly conserved. The histograms of branching angle, and branch length and thickness gradient can be described using lognormal and exponential distributions, respectively.

Conclusions

This unique study presents data to characterize mechanically important structural roots, which will help link root architecture to the mechanical behaviors of root structures.

Introduction

Tree roots develop their unique architectures through interactions with environments during their growth. The architectural characteristics of a root system not only affect the uptake and transport of water and nutrients, but also determine root anchorage through mechanical interactions with the surrounding soil. Most specifically, the tree root system can be represented by a combination of main structural roots and fine roots. The main structural roots possess about 90% of biomass forming the mechanical support system of plants while fine roots primarily control uptake of soil resources (Bohm 1979; Vogt and Persson 1991). The descriptions of architecture considered in this investigation are focused on the structural roots, as its goal is to develop descriptions of tree root architecture that will facilitate making connections between tree root architecture and mechanical root anchorage.

The architecture of structural roots can be described in several ways depending on the purpose and mechanisms of interest (Tobin et al. 2008; Reubens et al. 2007; Danjon et al. 2013; Dupuy et al. 2005; Danjon and Reubens 2008; Oppelt et al. 2001; Collet et al. 2006). Table 1 lists some frequently used descriptors and geometric parameters for architectural description of roots. Architecture is often described in terms of topological characteristics, with an emphasis on structure connectivity, independent from the geometry. Common topology parameters are altitude (the number of branching orders traversed from the trunk to root tips), magnitude (the total number of root tips), and topological index (the logarithmic ratio of these) (Berntson 1994; Fitter 2002). These parameters allow assessment of the system topology on a spectrum between the extremes of "*herringbone*" and "*dichotomous*" structures (Dupuy et al. 2003; Fitter 1987). The herringbone structure is characterized by major roots with lateral branching along them that have minimal further subdivision. The dichotomous structure is characterized by terminal branching with a parent root bifurcating into two child roots forking further down. However, the topological descriptions depend on assumptions about the geometry (diameters and orientations of the branches and sub-branches). As an example, both altitude and magnitude are altered just by changing the minimum diameter of root being considered.

Table 1
Commonly used architectural parameters

Parameter	*Definition*
Root volume	Volume of tree root system in the soil
Root length	Total sum of root length
Horizontal spread	Maximum horizontal distance
Rooting depth	Depth of the deepest root in a root system
Cross-sectional area	Area of cross-section (calculated from root diameter)
Allocation ratio (q)	Average ratio of the cross-sectional area of larger branch to the total cross-sectional area of all branch (if q is 1, herringbone and if q is 0.5, dichotomous)
Proportionality index (p)	Area ratio of before and after branching ($Area_{parent}/Area_{children}$)
Branching angle	Angle between parent root and children root
Root order or *Generation number*	Branching order of each root segment
Root fork number or *Total bifurcation number*	Total number of root bifurcations

Structural root architectures have been described in terms of qualitative categorizations. At the broadest level, many studies describe general categories of root system such as tap-, plate-, and heart-rooted systems (Dupuy et al. 2005). Tap root systems have prominent tap roots, which extend vertically downward from the base of the trunk, and much of the system's biomass is contained in it or originates from it. For example, early in the development of many tree species, including maritime pine, the tap root and its subsequent branching are dominant (Khuder et al. 2007). Plate root systems, such as that of Sitka spruce, have a larger proportion of lateral roots that extend shallowly from the base of the trunk (Coutts 1986). Heart root systems are described as having more variability in root inclination and more frequent branching like *platanus hybrida* (Danjon et al. 2005). Though these categorizations can be informed by quantitative observations, for many applications, including assessment of mechanical behavior, greater specificity is required.

Quantitative descriptions of structural root architecture include distribution of matter in space, allocation between different root types, and specific geometric observations. Danjon et al. (2005) have studied the coarse root architecture of mature *pinus pinaster*, assessing the biomass allocation to several categories of root type and location. They found that *pinus pinaster* primarily has a sinker root based system, wherein large lateral roots originate at the base of the trunk and extend mostly horizontally in the shallow reaches of soil, and along these roots periodic branches extend steeply downward. Danjon et al. (1999) have found that the biomass of roots located within the ZRT (zone of rapid taper), which primarily encompasses the shallow horizontal roots extending from the base of the trunk, is negatively correlated with the biomass of the taproot and other deep roots, indicating a trade-off in allocation necessitated by limited resources. They also observed that the main laterals tended to grow at a slight downward angle of about 15 degrees, and the second order roots originating from these roots had larger mean branching angles than successive roots of higher order. Lastly, the cross-sectional area of all roots near to the trunk was found to be similar to the mean stem cross-sectional area at ground level, suggesting an approximate conservation of cross-section of the proximal root network. Nonetheless, geometric descriptors for tree root systems can have wide variations with associated statistical distributions which still require further examination. Mechanical modeling and physiological growth modeling of tree roots requires such data measured from natural tree roots. Furthermore, there is a need for quantitative data and analysis of natural tree root architectures using descriptors that are expected to be relevant and useful in subsequent structural anchorage analyses.

This study explores the architectural characteristics of ten natural 3-year old orchard tree root systems (including Lovell, Marianna, and Myrobalan rootstocks) that were extracted from the ground by vertical pullout (Burrall et al. 2020). Table 2 lists bulk properties of the

model root systems, including the pullout capacities. Specifically, the Myrobalan rootstocks had the highest capacities, followed by Marianna and then Lovell. It was hypothesized that architecture likely played a role in producing these differences, and therefore a detailed assessment of the architectures was desired. Following pullout, the orchard tree roots were cleaned and then scanned with 3D photogrammetry. Full 3D models with ~ 1–2 mm resolution were constructed for each of the 10 root systems. These full 3D models are quantitatively examined and described using geometric parameters with statistical distributions. Within the broad range of parameters that could be evaluated, focus is placed on parameters expected to influence the mechanical interaction of the roots with surround soil and the overall anchorage performance during vertical pullout. The following geometric parameters are selected for analysis: root volume, root length, branching angles, branch length, root thickness, and root cross-sectional area (CSA). The resulting descriptors are expected to enable realistic modeling of root architecture and to facilitate linking the root architecture to the mechanical behaviors of root structures to suggest the most mechanically relevant parameter space for root system representation.

Table 2
Bulk properties for model tree roots

Symbol	*Lovell1*	*Lovell 2*	*Lovell 3*	*Lovell 4*	*Marianna 1*	*Marianna 2*	*Marianna 3*	*Myrobalan 1*	*Myrobalan 2*	*Myrobalan 3*
Species	Lovell	Lovell	Lovell	Lovell	Marianna	Marianna	Marianna	Myrobalan	Myrobalan	Myrobalan
Peak Pullout Capacity (kN)	5.7	7.5	4.3	4.8	8.0	9.9	6.5	10.7	16.4	12.9
Total Volume (cm^3) [a]	3268	3446	2378	3411	4673	4082	1983	4018	3756	2219
Total Surface Area (cm^2) [a]	6861	9058	5043	5770	9807	6804	4994	9021	6512	6730
Total length (cm) [b]	1871	3100	1274	1279	2462	1415	1112	1969	1463	1378
Trunk diameter (cm) [c]	8.2	8.6	7.4	8.3	8.2	8.2	7.2	6.3	7.6	6.6
Buried depth (cm)	58	39	35	61	36	52	58	38	65	63
Maximum hemisphere radius (cm) [d]	110	110	120	110	110	120	90	100	110	100
Number of generation	7	6	7	9	10	12	7	7	8	6
Fractal dimension for volume	1.27	1.09	1.11	1.33	1.53	1.19	1.17	1.35	1.37	1.06
Fractal dimension for area	2.03	1.92	1.73	1.69	1.76	1.42	2.16	1.61	1.61	1.66

Note. [a] Volume and surface area are calculated from STL format. [b] Total length is calculated from the skeletons. [c] The trunk diameter is estimated from the diameter of the maximum inscribed sphere. [d] Maximum hemisphere radius is equivalent to the distance from the trunk center at the ground surface.

Methods And Materials

Tree sample description

Ten root systems were subjected to vertical pullout in the UC Davis Plant Science Department teaching orchard (Burrall et al. 2020). The orchard trees, the scion and the rootstock, were selected for testing based on apparent differences in root architecture and perceived differences in anchorage performance. The scion (the upper part of the tree starting at the stem) is spliced onto the rootstock (which starts at the stem and includes everything beneath) at the nursery of origin before being planted at about one year of age.

Three-year old trees with the Lovell, Marianna, and Myrobalan rootstocks were selected to investigate variations in the root architecture. Younger root systems were anticipated to be too heavily influenced by their recent transplanting with not enough time to grow and manifest their permanent structural system, while older systems could have exceeded the pullout capacity of the test equipment. In total, four Lovell, three Marianna, and three Myrobalan rootstocks were tested. Details of the test program and their pullout capacities are described in Burrall et al. (2020).

3D model reconstruction

After extraction and cleaning, a photogrammetry survey of the extracted root system was conducted to construct 3D models of the root systems. Figure 1 shows all the reconstructed 3D root models used for analysis in this study. To develop the 3D models, each of the root systems were first fixed at the trunk base to a reference structure. Fine roots which were smaller than 5 mm diameter at the connection or shorter than 3 mm along the length, were trimmed from the system as these were too small to be reasonably captured with photogrammetry. A Nikon D3200 24-megapixel camera was used to take a total of 180 pictures of each root system. The photos were taken from 36 different angles and 5 different heights. The photogrammetry code, Metashape (Agisoft LLC, St. Petersburg, Russia), was used to stich images together and generate 3D models of the extracted root systems. These models were then re-scaled and aligned based on the reference structure and markers. Additional direct measurements of root diameters and position were also made using calipers and a laser distance measuring device, and were used to verify and correct the scaling of the 3D model. Finally, all above-ground parts of the reconstructed 3D models were removed.

Skeletonization

The 3D models were skeletonized to assess the distribution and architecture of the root systems. The skeleton tracks the root system with the root segments and defines the connectivity of the root segments. This skeletonization is conducted manually using a MATLAB code developed with a graphic user interface (GUI). Nodes are created by selecting points or pairs of points along the surfaces of the 3D meshes and then toggling segments to connect the vertices where appropriate. The x, y, z positions of the created nodes are then defined to be centered within the root branches or within the bifurcation joints. As a result, each tree root skeleton is composed of nodes and segments. The skeleton for each root includes the x, y, z positions of all the nodes as well as a connectivity matrix which indicates which nodes are connected to each other by root segments. Figure 2a shows the skeleton of Lovell 4, where the black spheres show the nodes and the black cylinders denote the root segments. The bifurcation nodes with the connectivity of three can be specified; black spheres and green spheres indicate the non-bifurcation nodes and the bifurcation nodes, respectively, as shown in Fig. 2a. The overlapped image of 3D model and skeletons of Lovell 4 confirms successful skeletonization (Fig. 2b).

Bulk property analysis

The bulk properties of the root architectures are characterized using the 3D models and their skeletons (Table 2). The total volume, total surface area, and buried depth are obtained from reconstructed 3D models as a format of the Standard Tessellation Language (STL) using Rhinoceros 5 (MacNeel et al., 2010). The root diameter is defined by employing the concept of local thickness, defined as the diameter of the maximum inscribed sphere within a 3D model, as shown in Fig. 3 (Adam, 2021). After the 3D mesh file is converted to image stacks with a voxel size of 1 mm, the local thickness is then calculated by using an ImageJ software plugin (Hildebrand and Rüegsegger, 1996; Fig. 3a), which requires an image stack as an input file (Adam, 2021). The local thickness value at a specific location from a root image stack indicates the diameter of the maximum inscribed sphere, which is related to the root diameter (Fig. 3a). Figure 3a shows some selected sliced images with the color-coded local thickness value of Lovell 4. Figure 3b shows a superimposed image of 3D model and spheres having the diameters of local thickness value, in which the sphere size represents the root diameter at the bifurcation points. Other quantifications of bulk properties include the total length, which is calculated as the sum of the branch length from the tree skeletons. In addition, variations in root volume and surface area with respect to the radial distance from the center of the trunk at the ground surface are computed.

Geometrical characterization of root architectures using skeletons

Figure 4 illustrates the definitions and methods used to compute the architectural parameters and branching characteristics, which include the branching angle, relative azimuthal angle, and branch length. In this study, the architectural characterization is performed based on the bifurcation nodes using the simplified skeletons, as described in Fig. 4b. All branches in the simplified skeletons can be divided into three categories, trunk root, main lateral root and remaining lateral root, based on their location and bifurcation generation. The trunk roots are manually identified from the skeletons, and the lateral roots that originate from the trunk roots are defined as the main lateral roots. All other roots are defined as the remaining lateral roots. The nodes connecting the trunk root branches are defined as the tap nodes. All other nodes are defined as lateral nodes. All the model roots have the tap nodes with the trunk roots, except for Marianna 2 (Fig. 1). For Marianna 2, there is no distinct trunk root, such that all branches and nodes are defined as lateral roots and nodes.

The nodes can be also indexed as non-bifurcation nodes, bifurcation nodes, and end nodes. The generation number of a branch is defined as the number of bifurcations, which is how many bifurcations exist from the branch's recent bifurcation back to the first tap node of the main trunk. This generation number increases incrementally each time it passes through one bifurcation node from the tap node to the end node. For instance, the generation number of a trunk root is one, that of a main lateral root is two, and the generation number of the remaining lateral roots starts from three.

Bifurcation produces two child roots from one parent root at the corresponding bifurcation node. The position of a child root can be specified relative to its parent root vector with its bifurcation node at the origin; accordingly, two kinds of relative angles can characterize the position of a child root — the branching angle and the relative azimuthal angle (Fig. 4). The branching angle is the angle between the child root and the parent root. Determination of the relative azimuthal angle requires transformation of the root position for consistent calculation of relative azimuthal angle. First, the bifurcation node of this root segment is translated to the origin. Second, the root segment is horizontally rotated in a x-y plane to align the parent root parallel to positive x-axis. Third, the segment is rotated in a x-z plane vertically to align the parent root with z-axis in parallel. Thereafter, the relative azimuthal angle is calculated as the angle between the positive x-axis and the projection of the child root to the x-y plane in a counter-clockwise direction.

The branch length and root diameter are also calculated. The branch length is calculated as the distance between two bifurcation points (Fig. 4). The root diameter at each node is determined as the diameter of the maximum inscribed sphere, which is equivalent to the local thickness value within 10 voxels from the node. Therefore, a set of 20 sliced images (10 above the node and 10 below the node) is used when the node is not positioned at the center within the root.

Results: Root Architectural Characteristics

Bulk properties of the model orchard tree roots

Table 2 summarizes the bulk architectural properties of the root models, which include the total volume, total surface area, total length, buried depth and the number of generations, among others. The model orchard trees have a similar trunk diameter of ~ 7–8 cm (Table 2). The total root volume ranges from 1,983 to 4,673 cm^3, with the total root volume increasing with an increase in the trunk diameter because the volume of the main trunk (tap root) comprises a large portion of the total volume (e.g., 30–50% of the root models). The total surface area and length are 4,994–9,807 cm^2 and 1,112–3,100 cm, respectively. The buried depths range from 38–65 cm; Lovell 2 and 3, Marianna 1 have shallow depths of ~ 35–40 cm while Lovell 4, Marianna 3 and 4 have depths as high as ~ 60 cm. The three year old trees bifurcate 7–10 times on average. As shown by these bulk properties, there are no clear distinct differences among the Lovell, Myrobalan, and Marianna species.

Figure 5 shows the cumulative volume and surface area versus the distance from the trunk center at the ground surface (or trunk top). A hemisphere with the center at the top of the trunk can be imagined; and, the volume and surface area of the root enclosed by the hemisphere are calculated as a function of the radius of the hemisphere. As shown in Fig. 5, the cumulative root surface area and volume increase as the hemisphere radius is increased. The maximum distance from the trunk top to the root tip is less than approximately 120 cm.

The slope of the relationship between root volume or surface area with its distance from the trunk top is related to the fractal dimension of the root architecture, as follows:

Root Volume or Area = $F \bullet R^{\tau}$, (1)

where R is the distance from the trunk top, F is a constant, and τ is the fractal dimension. Both the volume and the area show a bilinear trend with the distance from the trunk in log-log scale plots, and the region with the hemisphere radius from 10 cm to 30 cm, which is close to the trunk with active bifurcation, is chosen to determine the fractal dimension. It is found that the fractal dimension ranges 1.1–1.5 for the volume, and 1.6–2.2 for the surface area (Fig. 5). The fractal dimensions for the root volume are consistent with the previously reported values; *e.g.*, 1.17–1.66 for the coarse root systems of *Grewia flava, Strychnos cocculoides, Strychnos spinosa, Vangueria infausta* and 1.85 for the 6-week old tomato root system (Eshel, 1998; Oppelt et al. 2000). It is noted that this study uses the hemisphere-counting method while those previous studies used the box-counting method for the fractal dimension analysis. To the authors' knowledge, there is no reported data on the fractal dimension for the surface area.

Angles of branches at bifurcation nodes

Root grow and extend through bifurcations. When bifurcation occurs at a node, two child roots grow from one parent branch. From the perspective of the bifurcation node, two types of relative angles with respect to the parent root can describe the direction of the child roots in three dimensions: the branching angle and the relative azimuthal angle between the parent root and one of the child roots. Therefore, at every bifurcation, two branching angles and two relative azimuthal angles are defined for two child roots.

Figure 6a presents the branching angle values determined from the model roots, and Fig. 6b shows the average values with associated standard deviations. When the parent root is vertical to the ground, a branching angle of 0° indicates the child root that grows down vertically and parallel with the parent root. A branching angle between 0° and 90° means that the child root grows diagonally down, and a branching angle between 90° and 180° corresponds to a child root that grows upwards toward the ground surface. The main lateral roots at a generation of 2 have the greatest branching angle, with a mean value close to 70°, implying that the child roots grow close to a horizontal direction (Fig. 6b). The branching angle decreases with an increase in generation number after generation 2, and the lateral roots at the last four generations have average branching angles between 10–30° (Fig. 6b). This indicates that the lateral roots at later generations bifurcate almost in parallel with minimal branching angles between the parent and child roots. This trend is consistent with previous studies with *A. lenticularis, A. nilotica, A. procera, D. sissoo, P. dulce, S. grandiflora, C. fistula*, and *S. cumini* (e.g., Chaturvedi and Das 2003), in which the primary roots have the greater branching angles than the secondary roots, and hence spreading of the primary roots is greater than that of the secondary roots.

The histograms of branching angles of entire root systems can be captured with lognormal distributions, as shown in Fig. 7. The mean branching angle for the trunk roots ranges from 35° to 66° for the main lateral roots. Most importantly, the lognormal distributions fitted to the data show that the main lateral branching angles are generally significantly larger than for the remaining laterals, resulting in radial extension away from the trunk axis.

Figure 8 shows the histogram of relative azimuthal angles for all child branches at all bifurcation points. The distribution reveals that the relative azimuthal angles roughly show a uniform distribution from 0° to 360°. This implies that the cardinal directions of bifurcated child roots are close to random regardless of root types (i.e., trunk, main lateral, and remaining lateral roots).

Branch length of roots

Figure 9 depicts the branch lengths and their mean values of all the model roots as a function of generation number. As mentioned before, the branch lengths are determined as the distance between the bifurcation nodes from the root skeletons. The branch lengths of the trunk roots are the shortest, mostly less than 10 cm (Fig. 9a). This implies frequent bifurcations over the course of tap root growth; on average, tap roots bifurcate every 1.6 cm. From the second generation (Generation 2), the branch length significantly increases, showing a range of average values between 10–30 cm (Fig. 9b).

Figure 10 shows the histograms of branch length values from all the root models. The results can be reasonably fitted with exponential distributions with the mean values differing depending on the root classification. The roots having a generation number greater than 2 have the greatest mean value of 21 cm (Fig. 10c) while the main lateral and trunk roots have values of 17.6 and 1.6 cm (Figs. 10a and 10b), respectively. This is consistent with the root growth patterns of the orchard trees, in that the roots grow longer before bifurcation for effective lateral coverage as they grow further away from the trunk. The 3D models shown in Fig. 1 visually corroborates this pattern.

Distribution of root diameters: local thickness analysis

The root diameters are examined based on the diameters of the maximum inscribed spheres (MIS) that fit within the 3D models. This MIS diameter is also called the local thickness (LT). Figure 11 shows the cumulative distributions of root diameters for the model roots. Note that the median value of the root diameter, *LT50*, corresponds to the 50th percentile of root volume fraction. The median root

diameters range from 14.5 to 33.5 mm. Lovell 4 shows the maximum *LT50* of 33.5 mm while Lovell 2, Myrobalan 3, and Marianna 3 have the minimum *LT50* of 14.5 mm. Table 3 summarizes local thicknesses of roots. Particularly, the ratio of *LT60* to *LT10* can be used as an indicator to root diameter variations, how broadly the root diameters are spread. Similarly, in a discipline of geotechnical engineering and soil mechanics, the coefficient of uniformity, Cu, for the grain size distribution is defined as the ratio of *D60* to *D10*, and it has long been used as an engineering indicator to how widely the grain size varies for a given soil. The analysis reveals that the coefficient of uniformity (Cu) of the model roots, defined as *LT60*/*LT10* in this study, ranges from 2.7–5.6.

Table 3
Summary of local thickness

Symbol	*Lovell 1*	*Lovell2*	*Lovell3*	*Lovell4*	*Marianna 1*	*Marianna 2*	*Marianna 3*	*Myrobalan 1*	*Myrobalan 2*	*Myrobalan 3*
LT10	5.5	5.5	6.5	7.5	6.5	8.5	5.5	7.5	7.5	3.5
LT30	12.5	9.5	11.5	17.5	11.5	17.5	9.5	11.5	11.5	8.5
LT50	21.5	14.5	19.5	33.5	19.5	25.5	14.5	16.5	16.5	14.5
LT60	30.5	20.5	27.5	39.5	27.5	33.5	22.5	20.5	20.5	17.5
LT90	79.5	85.5	68.5	78.5	69.5	57.5	70.5	38.5	38.5	32.5
Cu [a]	5.55	3.73	4.23	5.27	4.23	3.94	4.09	2.73	2.73	5

Note: [a] The coefficient of uniformity in root thickness Cu is defined as LT60/LT10, which represents the variability in thickness. The Cu value of 1 indicates that the root thickness is uniform. Greater Cu indicates greater variation of root thickness.

The local thickness gradient is estimated using the local thickness values at two bifurcation nodes and the distance between two bifurcation nodes, *i.e.*, $\nabla LT = (LT_1 - LT_2)/L_2$. Figure 12a shows the local thickness gradient ∇LT with respect to the branch length L_2. The local thickness gradient decreases with an increase in the branch length, and all ∇LT values are positive. The result also shows that majority of ∇LT values are smaller than 0.5. Figure 13 shows the histograms of local thickness gradients for trunk, main lateral, and remaining lateral roots of entire root models, and they are described with the exponential distributions. The mean values of ∇LT for the trunk and main lateral roots are 0.35 and 0.32, respectively. In contrast, the mean ∇LT is 0.1 for remaining lateral roots. This result demonstrates that the root diameter decays at a significantly faster rate near the trunk. It is worth noting that the trunk roots and main lateral roots (generations 1 and 2) have roughly similar mean values of ∇LT, while their mean branch lengths have large differences (1.6 cm versus 17.6 cm, as denoted in Fig. 10).

The root cross-sectional area ratio at a bifurcation node is defined as the square of local thickness $((LT_2^2 + LT_3^2)/ LT_1^2)$. Such area ratio allows examination on the conservation of cross-sectional areas of a root across bifurcations. The area ratio is equivalent to the reciprocal of the proportionality index (p). Figure 12b shows the area ratio with respect to the mean branch length $((L_2 + L_3)/2)$. Herein, the area ratio is estimated with the main lateral roots and the lateral roots while the trunk root less than 3 cm long and the end branch are excluded. In most instances, the area ratio is close to 1, with most values ranging between 0.9 and 1.2, which implies the conservation of area across a bifurcation. This agrees with the pipe stem theory, which contends that this hydraulic architecture naturally evolves to preserve cross-sectional areas for efficient water and nutrient transport (Oppelt et al. 2001; Van Noordwijk et al. 1994). In addition to natural variability, there can be deviations in the hydraulic architecture from the external diameter owing to the thickness of non-conducting material encasing the root (Danjon et al. 1999, 2013; Coutts 1983). There are some cases where the area conservation is less than 1, and this low area ratio is more frequent as the branch length increases. This is simply because this area ratio estimation measures the thickness at the bifurcation nodes, therefore, the long branch length between the bifurcation nodes renders underestimation of the area ratio particularly. That is, the next bifurcation nodes (LT_2 and LT_3) are located too much far away from the current bifurcation node (LT_1).

Discussion

Implication to mechanical pull-out resistance of roots

Load transfer through a root system and into the soil is complex and varies for a wide range of conditions and structures. In particular, anchorage capacity is directly related to the architecture of the roots that are in contact to the soil where the transfer of force takes

place. Therefore, a connection between the root architecture and anchorage behavior requires characterization of the architecture in a manner that relates to the mechanical aspects of the system. The extracted root systems are characterized in a statistical manner, which capture the variations of architectural parameters and describe where the structure is present within the soil and how the structure is connected to the trunk (which is loaded in tension during pullout). The branching angle and azimuthal angle show the direction in which the root branches grow. The branch length and generation number indicate how rapidly the root bifurcates or divides and how the size of the elements is allocated between the parent and child roots. The root branch diameters as well as the branch length are relevant to both structural stiffness and contact surface area to the soil.

Results from our previous study in Burrall et al. (2020) suggest that differences in the root architecture can help explain differences in the mechanical pull-out responses. Primarily, the spatial distribution of thick structural roots, which can be described through a combination of branch length, branch angle, and diameter allocation aforementioned, plays a significant role in load transfer to the soil that provides support through frictional resistance. For an instance, Myrobalan 2 had the pullout capacity per volume of 4,364 kN/m^3 and Myrobalan 3 had the pullout capacity per volume of 4,326 kN/m^3, whereas Lovell 1 had the pullout capacity per volume of 1,751 kN/m^3 and Lovell 4 had the pullout capacity per volume of 1,406 kN/m^3 (see Table 2). The differences in material efficiency (capacity per volume) between Myrobalan and Lovell root systems is significant and it is not fully explained by differences in average depth and soil strength. The concave-up shape of the Myrobalan root systems significantly contributed to the greater pull-out resistance. Such root systems appeared to mobilize the more distal roots more effectively. In contrast, a thick trunk and an overconcentration of large, stiff roots near the trunk produced a pronounced block failure of the surrounding soil through group interaction, by which the pull-out resistance was comparatively small (*e.g.*, Lovells). Further investigation into the precise manner of the connection between the architectural variables and the mechanical behavior is needed.

Implication to architectural modeling of root growth: L-system modeling

The parameters measured in this study are chosen to realistically represent the characteristics of structural root systems. Statistical assessment of geometric quantities, such as branch length (inter-node length), branching angle, and local root thickness, provides most of the information necessary to define the extent and interconnectivity of structural roots. The presented analyses suggest that a wide range of structures and topologies can be realistically recreated by using relatively few parameters with a simple set of rules if the geometry is managed appropriately.

Full description of root architecture requires the elongation rate (or length), branching interval, branching angle, growth tortuosity, and gravitropism for each order (or generation) of root (Dupuy 2010). As an alternative to the above geometric descriptor-based approach, a fractal model that defines the architecture based on approximate rules of proportionality, such as allocation rules at branch points and scaling of lengths and branching angles, can be used (e.g., Van Noordwijk 1994). This fractal model is particularly well-suited to capture the architecture of roots with self-repeating patterns. Most importantly, the patterns in branching and diameter distributions in the current study show significant difference between the trunk and main laterals versus the remaining lateral roots. Thus, variation of characteristics between the initial stage and the remaining stages should be incorporated.

L-system modeling is a powerful formulation to store or represent a larger or more complicated structure in a compact manner through the use of reproduction rules (Prusinkiewicz 1999). It is a fractal model (Van Noordwijk, 1994) that also facilitates the use of different root types or stages with corresponding patterns and distributions in the case of stochastic modeling. One modeling method might look like the following: a parent root extends for some branch length sampled from the measured distributions and then divides, at which the child root diameters are sampled from the measured distribution of local thickness allocation, and the directions are sampled from the distributions of branch angle and azimuthal angle. For the most part, the required geometric parameters can be sampled directly from the distributions obtained in this study, at each decision point to develop a full system. Repeating this process can enable growth simulation of a simple root system while preserving the mechanically important structural characteristics. Our result places a particular emphasis on variations in architectural and geometrical parameters which will aid in more realistic modeling of root architectures. The statistical results do not explicitly contain physiological relation among the parameters, thereby, the values are not auto-correlated. Therefore, the root architecture modeling based on random sampling will have limitations in modeling the self-supervised growth of natural tree roots. Further refinement, such as the assessment of multivariate correlations may be required and it would facilitate this root growth simulation to abide by baseline physiological and physical limits, for instance, no extension above the ground surface or inward growth into oneself. Nevertheless, results of such simulations would allow assessing of the range of possible root architectures, facilitating parametric study of a range of possible architectures, and identifying further characteristics required to determine particular

architectures. Resulting patterns could then be explored either through numerical modeling or physical testing, with explicit control over the input characteristics.

Conclusion

This study examines the structural root architectures of ten orchard trees (Lovell, Myrobalan, Marianna species) using the reconstructed 3D models with an emphasis on the statistical distributions of geometric parameters. The 3D models allow measuring the total volume, surface area, and total length, while the skeletonized root models enable the determination of branching angle, relative azimuthal angle, and branch length at each bifurcation point, which can determine the direction and position of the child roots at every node. The main findings are as follows:

- The model roots of the chosen three species only show minimal difference in bulk properties such as the trunk diameters, buried depth, and generation number, though their total volume ranges from 1,983 to 4,673 cm^3 and the total surface area varies from 4,994 to 9,807 cm^2. The fractal analysis shows the fractal dimension of 1.1–1.5 for the volume growth, and 1.6–2.2 for the surface area growth.
- The analysis reveals that the patterns in branching and diameter distributions show significant difference between the trunk and main laterals versus the remaining lateral roots. In particular, the branching angle decreases with an increase in the generation number. Specifically, the main lateral roots have the greatest branching angle with the greatest extent of spreading while the lateral roots near the end tips show the smallest branching angle, growing more or less in parallel with the parent root. The histograms of branching angles show lognormal distributions. Meanwhile, the relative azimuthal angles show a fairly uniform distribution, which implies that the cardinal directions of bifurcated child roots are quite random.
- The branch lengths show exponential distributions, where the trunk roots are the shortest with a mean value of 1.6 cm, while the remaining roots have the greatest length with a mean value of 21 cm. The result indicates that the roots bifurcate more frequently near the trunk and they grow longer for effective lateral coverage when they are further from the trunk.
- The local thickness analysis enables quantification of the distributions of root diameters. The median root diameters range from 14.5 to 33.5 mm and the coefficient of uniformity in root diameter (Cu = LT60/LT10) ranges from 2.7–5.6. The local thickness gradient analysis indicates that the root diameter decays at a significantly faster rate near the trunk than in the remaining lateral roots. The local thickness gradient decreases with an increase in the branch length with the exponential distributions.
- The cross-sectional area analysis demonstrates that the area ratio across a bifurcation remains mostly close to 1, ranging between 0.9 and 1.2. This corroborates the pipe stem theory which states that the hydraulic architecture tends to preserve cross-sectional areas for efficient water and nutrient transport.
- The architectural parameters chosen in this study represent the characteristics of root systems most relevant to its mechanical behavior. This information helps explain the mechanical responses of the root systems, for an instance, a greater spread of lateral roots versus an overconcentration of large, stiff roots near the trunk.

This study presents unique data on statistical variations in architectural and geometrical parameters of tree roots, which provides essential information necessary to define the extent and interconnectivity of mechanically important structural roots. The simulation of root systems with such information would allow production of a wide range of possible root architectures, bridging the root architecture to the mechanical behaviors of root structures, and providing better understanding on mechanical interactions of root systems with surrounding soils.

Declarations

Acknowledgements

This research was supported by the National Research Foundation of Korea (NRF) grant funded by the Korean government (Ministry of Science, ICT & Future Planning) (No.2020R1A2C4002358) and the Engineering Research Center Program of the National Science Foundation (NSF) under NSF Cooperative Agreement EEC-1449501. Any opinions, findings and conclusions or recommendations expressed in this material are those of the authors and do not necessarily reflect those of the NSF.

Competing Interests

The authors have no relevant financial or non-financial interests to disclose.

Author Contributions

All authors contributed to the study conception and design. Material preparation, data collection and analysis were performed by Min-Kyung Jeon and Matthew Burrall. The first draft of the manuscript was written by Min-Kyung Jeon, Matthew Burrall, and Tae-Hyuk Kwon. All authors commented on previous versions of the manuscript. All authors read and approved the final manuscript.

Data Availability

All data, models, or code that support the findings of this study are available from the corresponding author upon request.

References

1. Adam A (2021) Mesh voxelisation (https://www.mathworks.com/matlabcentral/fileexchange/27390-mesh-voxelisation), MATLAB Central File Exchange. Retrieved May 3, 2021
2. AgiSoft PhotoScan Standard (Version 1.5.0) (Software) (2018) Retrieved from http://www.agisoft.com/downloads/installer/
3. Berntson G (1994) Modelling root architecture: are there tradeoffs between efficiency and potential of resource acquisition? New Phytol 127:483–493
4. Böhm W (1979) Root Ecology and Root Physiology. Methods of Studying Root Systems. Springer
5. Burrall M, DeJong JT, Martinez A, Wilson DW (2020) Vertical pullout tests of orchard trees for bio-inspired engineering of anchorage and foundation systems. Bioinspir Biomim 16:016009
6. Chaturvedi O, Das D (2002) Studies on rooting patterns of 5-year-old important agroforestry tree species in North Bihar, India. Forests trees and Livelihoods 12:329–339
7. Collet C, Löf M, Pagès L (2006) Root system development of oak seedlings analysed using an architectural model. Effects of competition with grass. Plant Soil 279:367–383
8. Coutts M (1983) Root architecture and tree stability. Tree root systems and their mycorrhizas. Springer
9. Coutts MP (1986) Components of tree stability in Sitka spruce on peaty gley soil. Forestry: An International Journal of Forest Research 59(2):173–197
10. Danjon F, Bert D, Godin C, Trichet P (1999) Structural root architecture of 5-year-old Pinus pinaster measured by 3D digitising and analysed with AMAPmod. Plant Soil 217:49–63
11. Danjon F, Fourcaud T, Bert D (2005) Root architecture and wind-firmness of mature Pinus pinaster. New Phytol 168:387–400
12. Danjon F, Khuder H, Stokes A (2013) Deep phenotyping of coarse root architecture in R. pseudoacacia reveals that tree root system plasticity is confined within its architectural model. PLoS ONE 8:e83548
13. Danjon F, Reubens B (2008) Assessing and analyzing 3D architecture of woody root systems, a review of methods and applications in tree and soil stability, resource acquisition and allocation. Plant Soil 303:1–34
14. Dupuy L, Fourcaud T, Lac P, Stokes A (2003) Modelling the influence of morphological and mechanical properties on the anchorage of root systems. Universität Karlsruhe
15. Dupuy L, Fourcaud T, Stokes A (2005) A Numerical Investigation into the Influence of Soil Type and Root Architecture on Tree Anchorage. Plant Soil 278:119–134. doi: 10.1007/s11104-005-7577-2
16. Dupuy L, Gregory PJ, Bengough AG (2010) Root growth models: towards a new generation of continuous approaches. J Exp Bot 61(8):2131–2143
17. Eshel A (1998) On the fractal dimensions of a root system. Plant Cell Environ 21:247–251
18. Fitter A (1987) An architectural approach to the comparative ecology of plant root systems. New Phytol 106:61–77
19. Fitter A (2002) Characteristics and functions of root systems. In Plant roots: the hidden half. Third edition. Weisel, Y. Eshel, A. and Kafkafi, U. eds., Marcel Dekker, New York pp 15–32
20. Hildebrand T, Rüegsegger P (1997) A new method for the model-independent assessment of thickness in three-dimensional images. J Microsc 185:67–75
21. Khuder H, Stokes A, Danjon F, Gouskou K, Lagane F (2007) Is it possible to manipulate root anchorage in young trees? Plant Soil 294:87–102
22. MacNeel, R. et al. (2010). Rhinoceros 3D, Version 5.0. Robert McNeel & Associates,Seattle, WA

23. Oppelt AL, Kurth W, Dzierzon H, Jentschke G, Godbold DL (2000) Structure and fractal dimensions of root systems of four co-occurring fruit tree species from Botswana. Ann For Sci 57:463–475
24. Oppelt AL, Kurth W, Godbold DL (2001) Topology, scaling relations and Leonardo's rule in root systems from African tree species. Tree Physiol 21:117–128
25. Prusinkiewicz P (1999) A look at the visual modeling of plants using L-systems. Agronomie 19:211–224
26. Reubens B, Poesen J, Danjon F, Geudens G, Muys B (2007) The role of fine and coarse roots in shallow slope stability and soil erosion control with a focus on root system architecture: a review. Trees 21:385–402
27. Tobin B, Čermák J, Chiatante D, Danjon F, Di Iorio A, Dupuy L, Eshel A, Jourdan C, Kalliokoski T, Laiho R (2007) Towards developmental modelling of tree root systems. Plant Biosystems 141:481–501
28. van Noordwijk M, Spek LY, de Willigen P (1994) Proximal root diameter as predictor of total root size for fractal branching models. Plant Soil 164:107–117

Figures

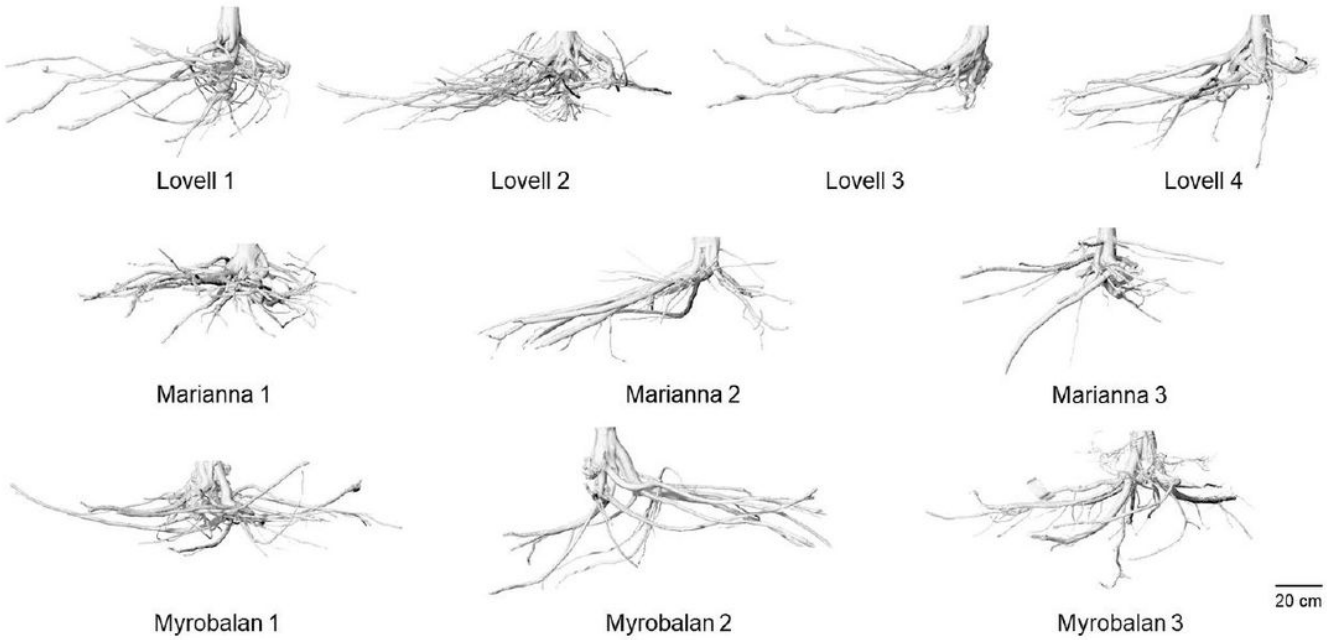

Figure 1

Reconstructed 3D models of tree samples.

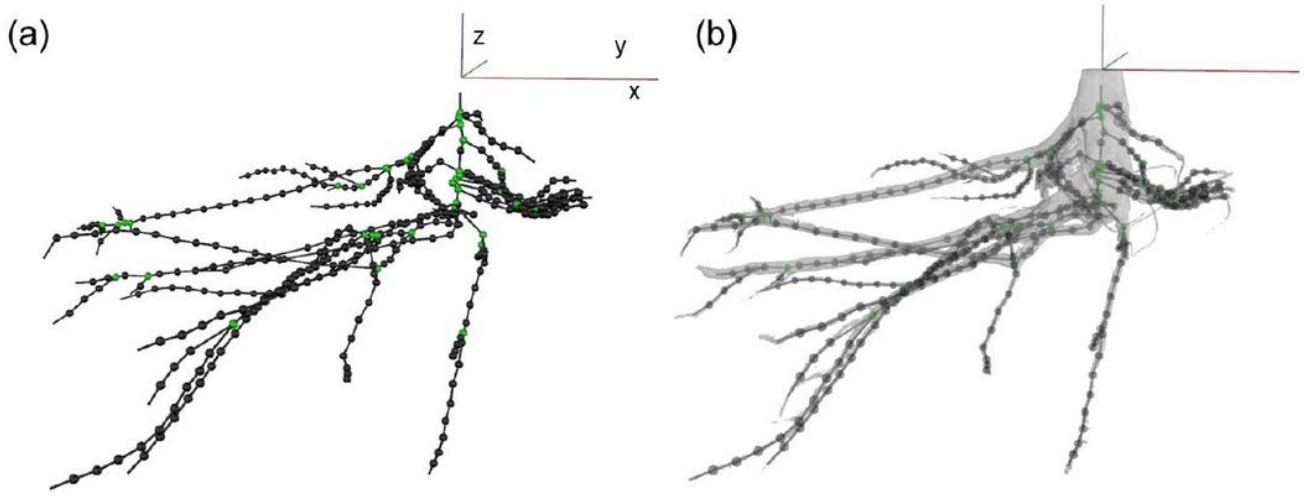

Figure 2

Skeletonized root model Lovell 4: (a) the skeleton of the root model Lovell 4, and (b) comparison of the full 3D model and the skeleton. Green and black spheres represent the bifurcation and non-bifurcation nodes, respectively. Black cylinders arethe root branches which connect two nodes.

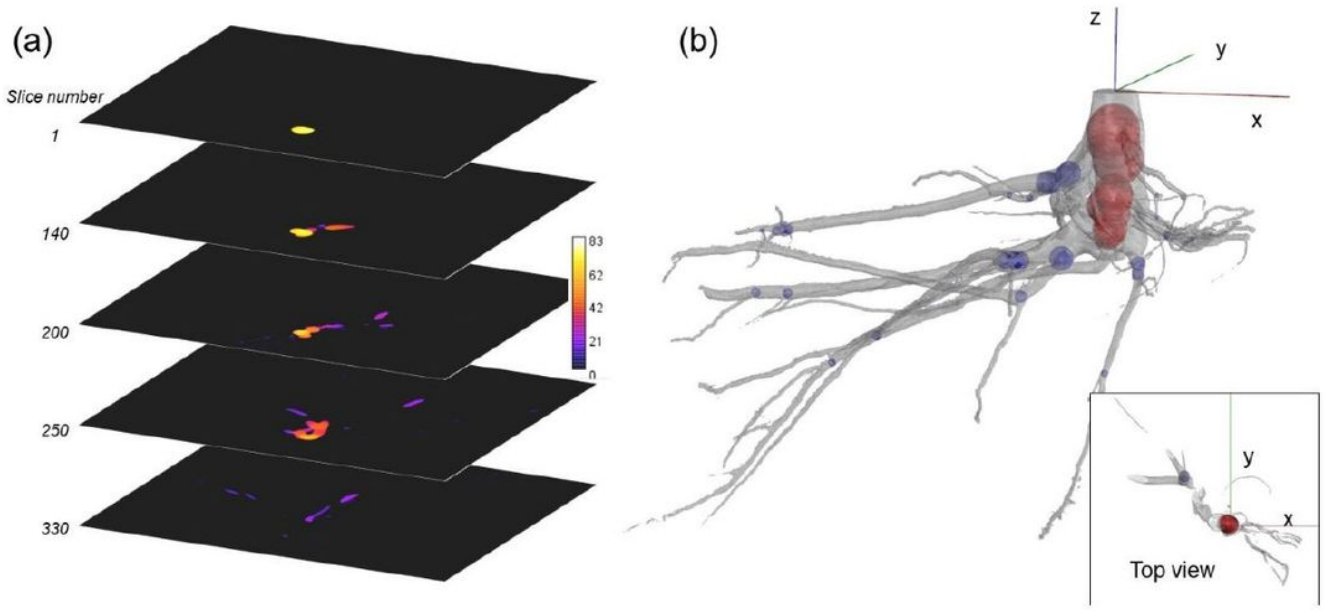

Figure 3

(a) Estimation of the maximum inscribed spheres in a stack of sliced images of Lovell 4. The local thickness value is described in color (mm). (b) The maximal inscribed spheres superimposed at the bifurcation nodes of full 3D model of Lovell 4. Note that red spheres indicate the maximal inscribed spheres at the tap nodes in the trunk root, and blue spheres at the lateral bifurcation nodes in the lateral roots.

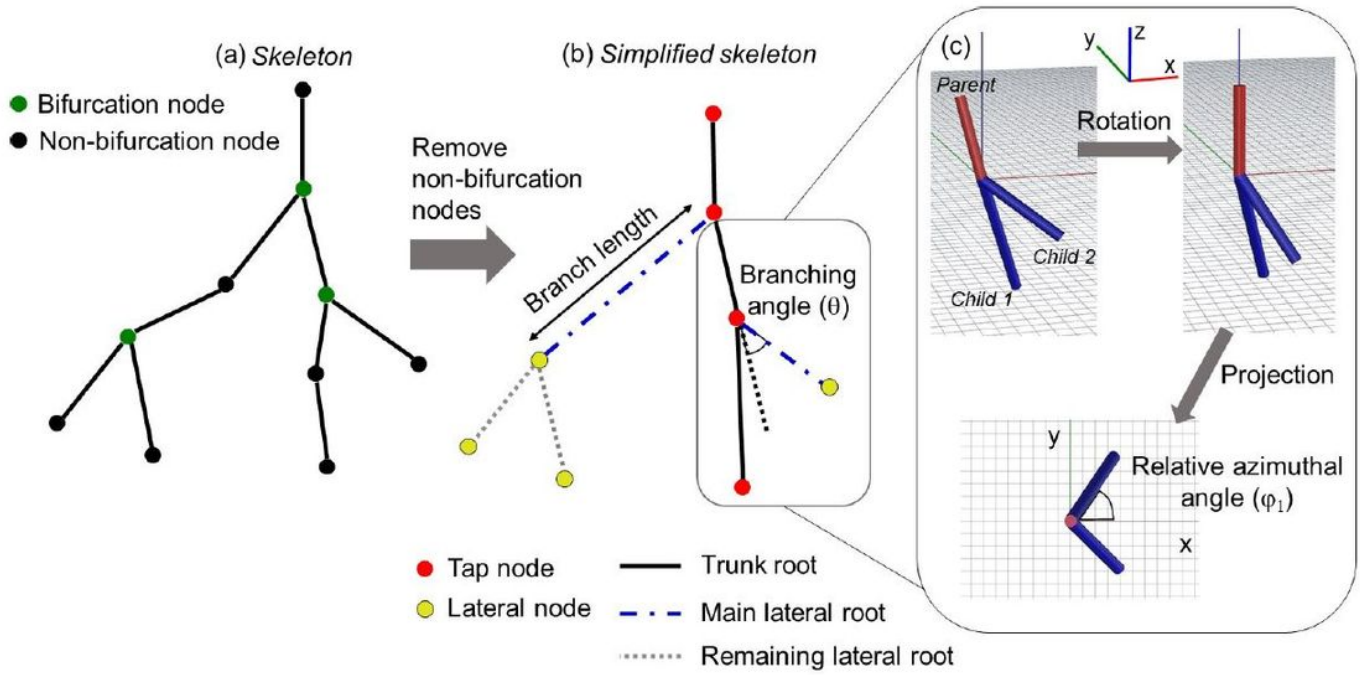

Figure 4

Definition of the architectural parameters from a skeletonized model.

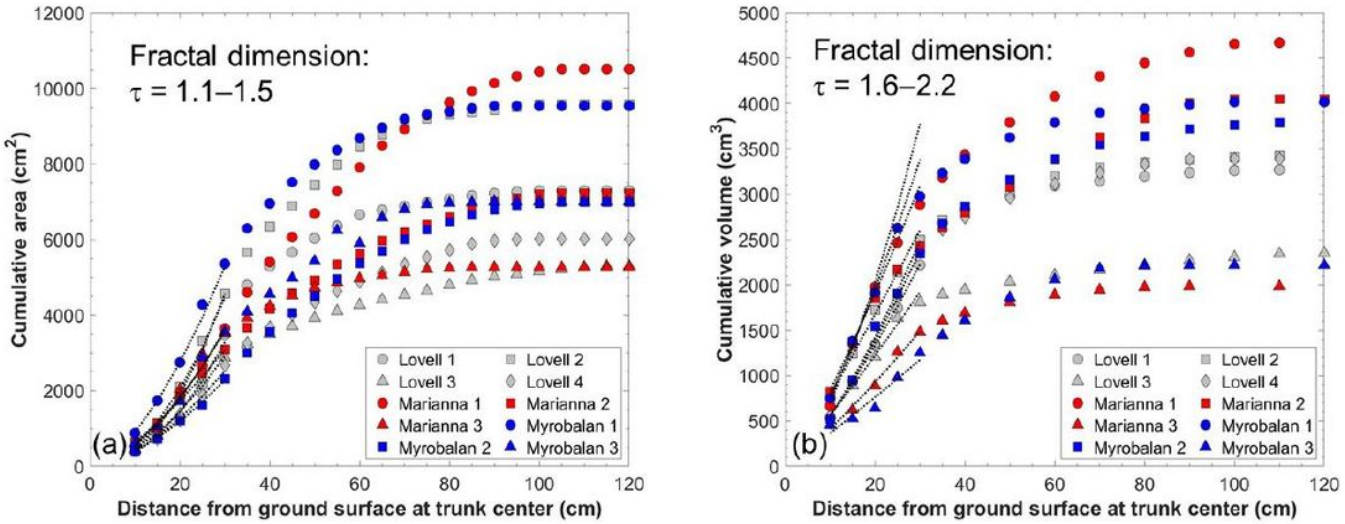

Figure 5

(a) Cumulative surface area and (b) cumulative root volume with respect to the radial distance from the trunk center at the ground surface. The fractal dimension τ is determined following the equation: Volume or Area = $F \cdot R^{\tau}$, where R is the radial distance from the trunk center at the ground surface.

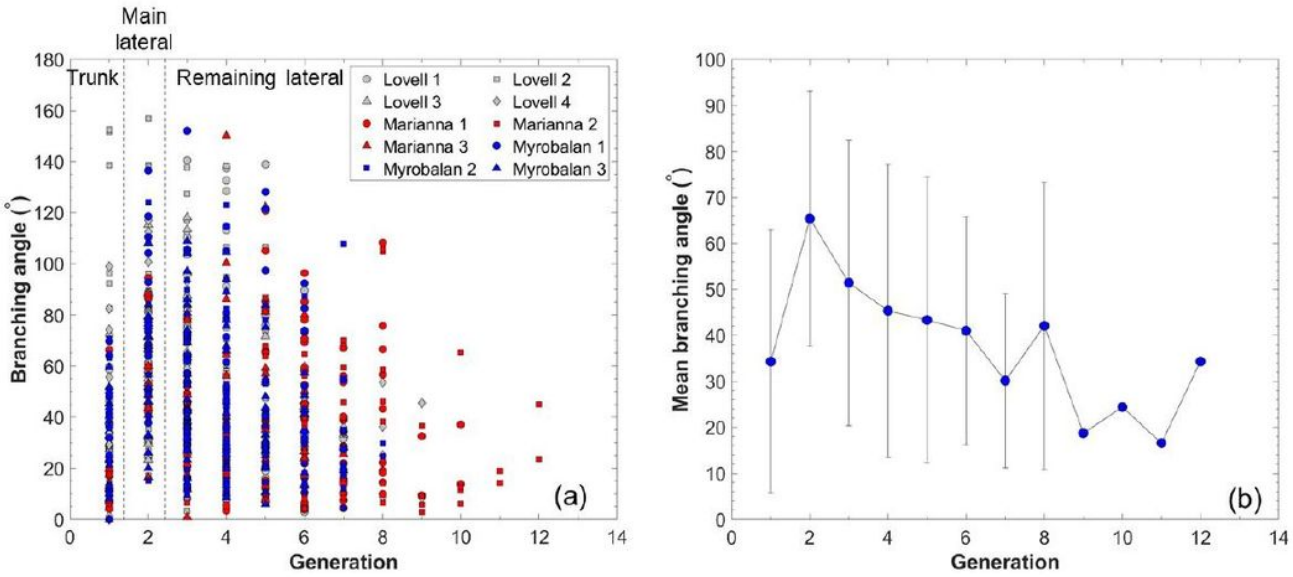

Figure 6

(a) Variations in branching angle, and (b) variations in mean branching angle with respect to the generation number. Generation of the trunk and the main lateral is 1 and 2, respectively. The error bars in (b) denote μ ± σ.

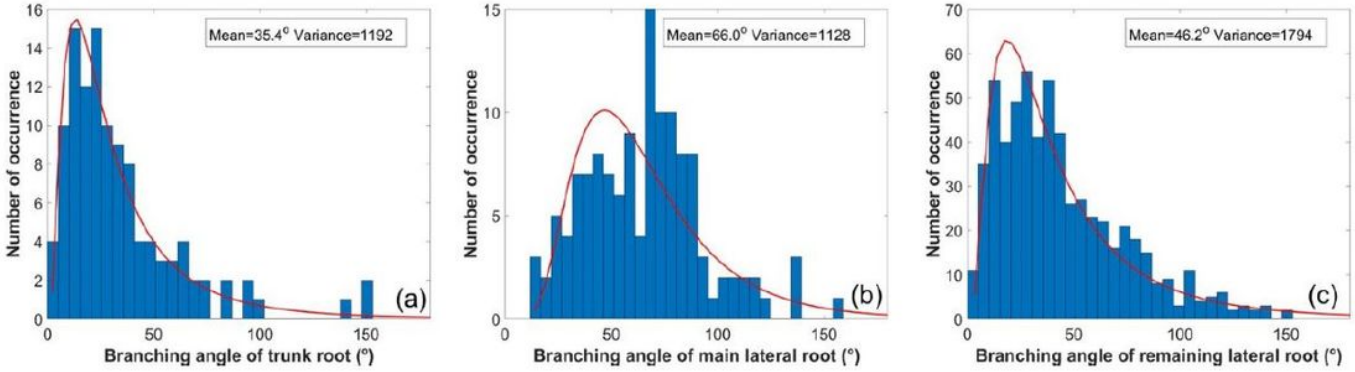

Figure 7

Histograms of branching angles: (a) trunk roots, (b) main lateral roots, and (c) remaining lateral roots. The means and variances are determined using lognormal distributions.

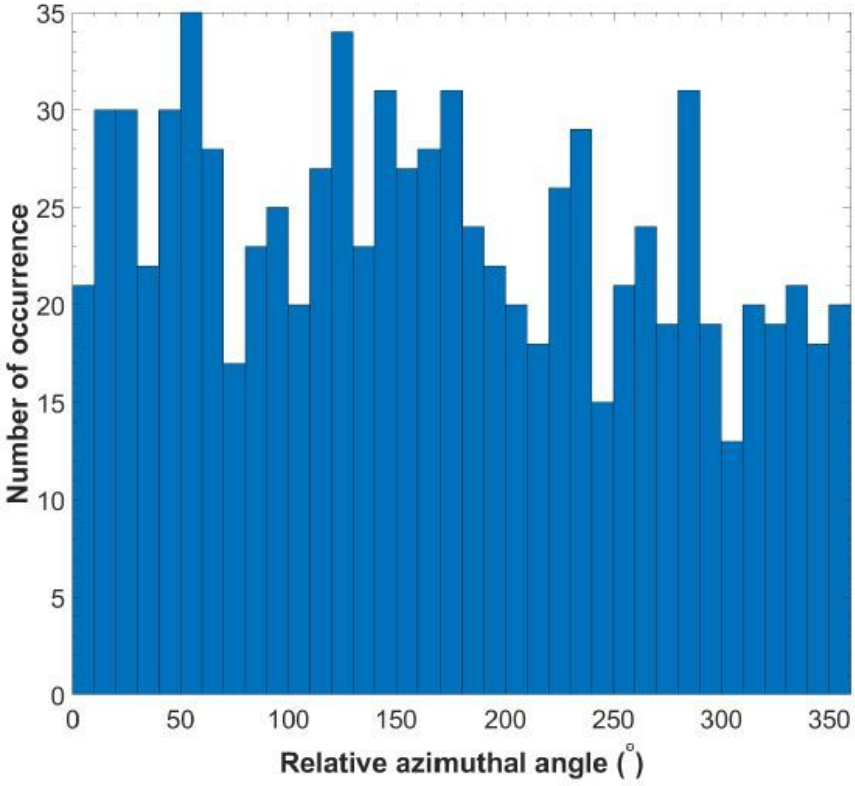

Figure 8

Histogram of relative azimuthal angles for child roots.

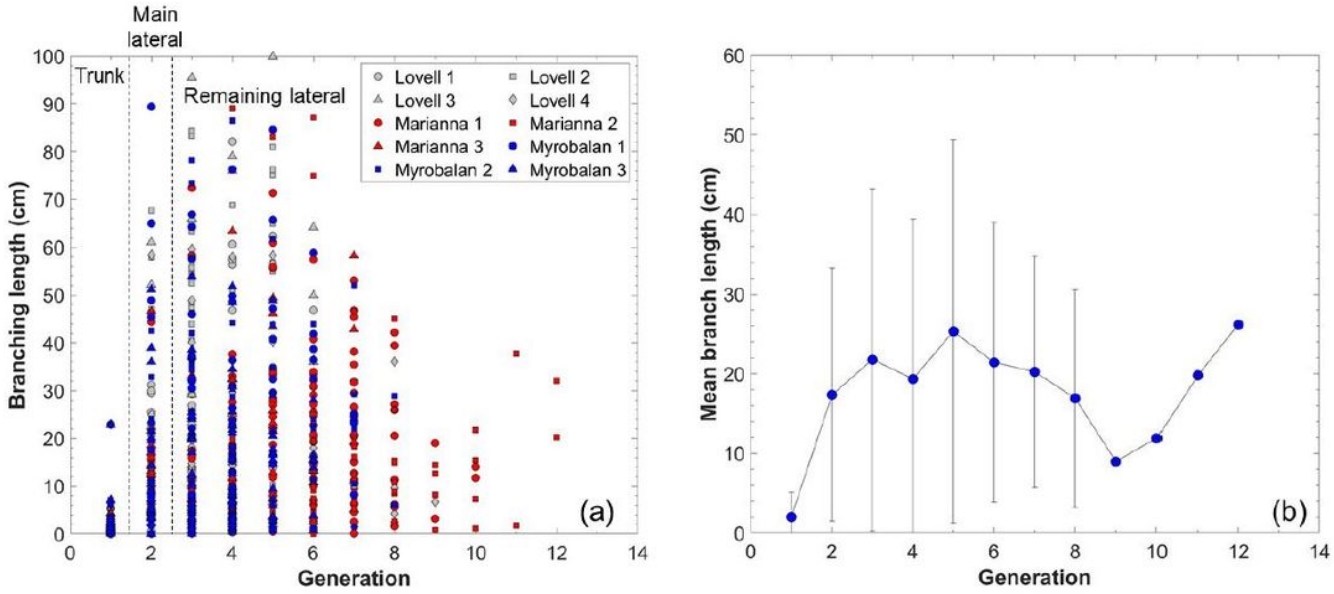

Figure 9

(a) Variations in branching length, and (b) variations in mean branching length with respect to the generations. Generation of the trunk and the main lateral is 1 and 2, respectively. The error bars in (b) denote μ±σ.

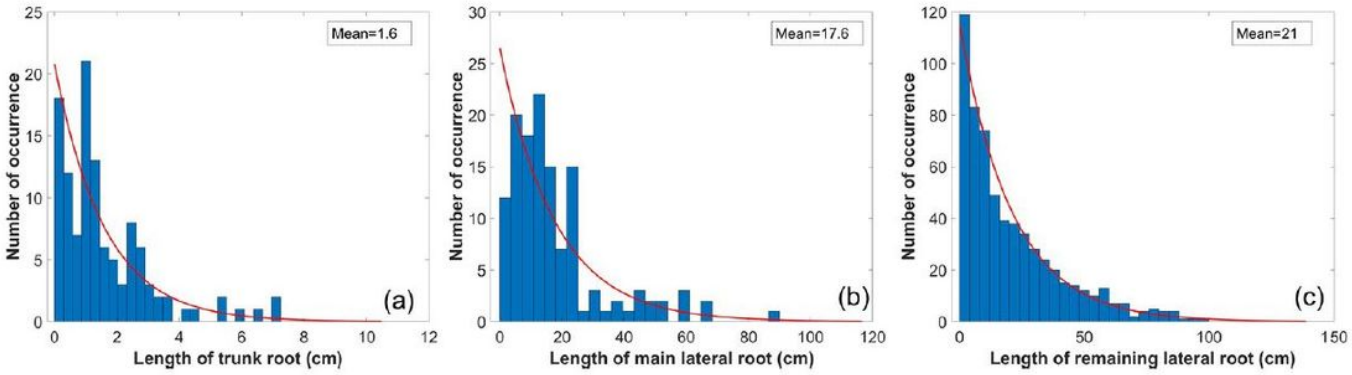

Figure 10

Histograms of branch lengths: (a) trunk roots, (b) main lateral roots, and (c) remaining lateral roots. The mean value is determined using exponential distributions.

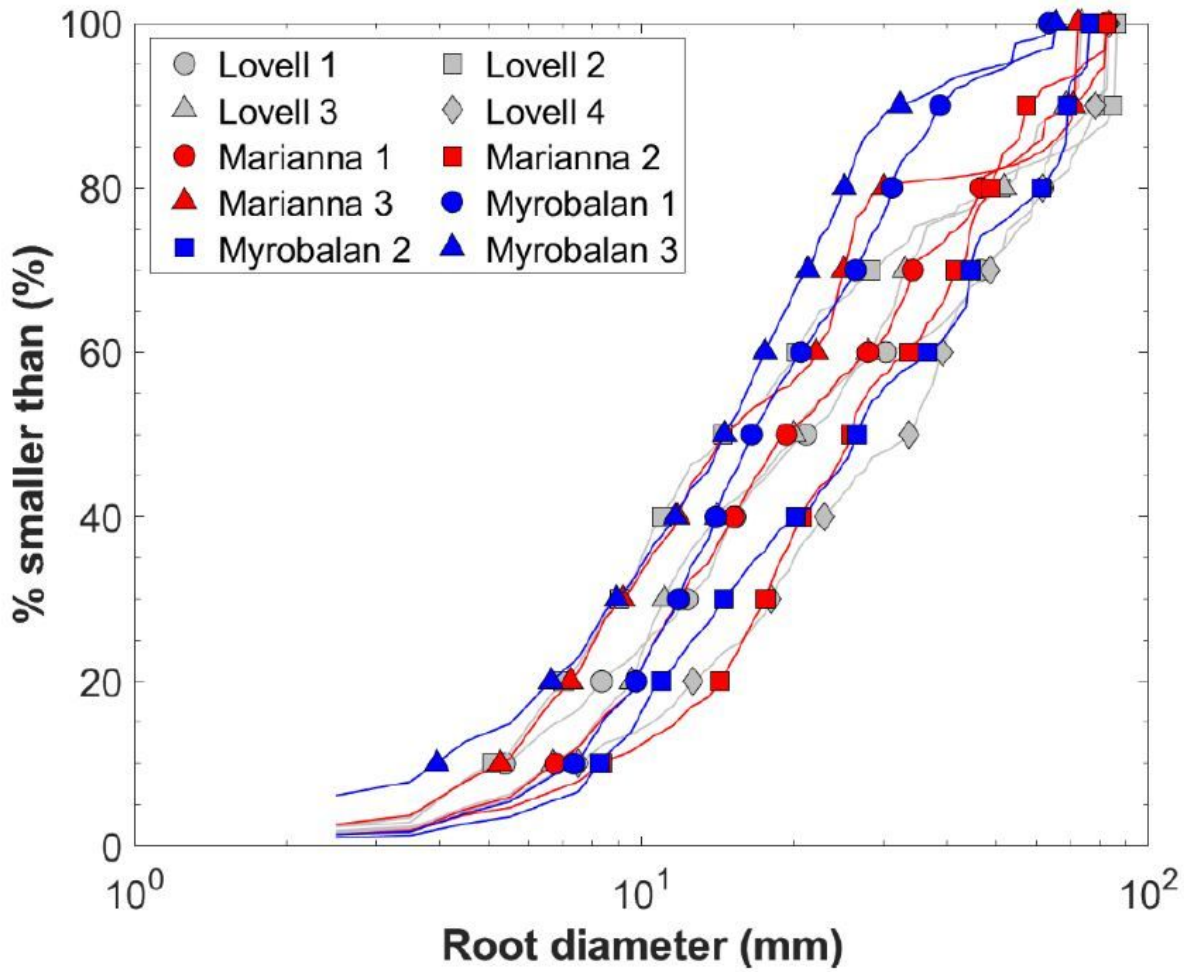

Figure 11

Cumulative distributions of the root diameters. The markers indicate the 10th percentiles of root volume fractions, e.g., LT70 means that 70% of the root volume is smaller than the corresponding diameter.

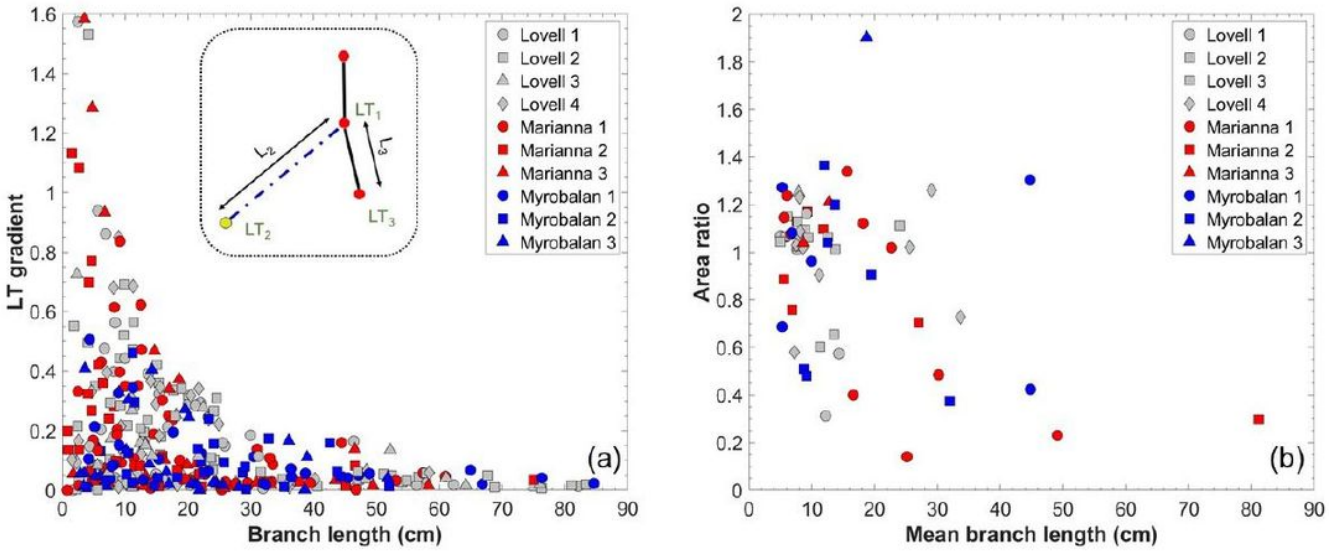

Figure 12

(a) Local thickness gradients and (b) area ratios with respect to the mean branch length. The local thickness gradient ÑLT is defined as (LT1 – LT2)/L2. The area ratio is defined as ((LT22+ LT32)/ LT12).

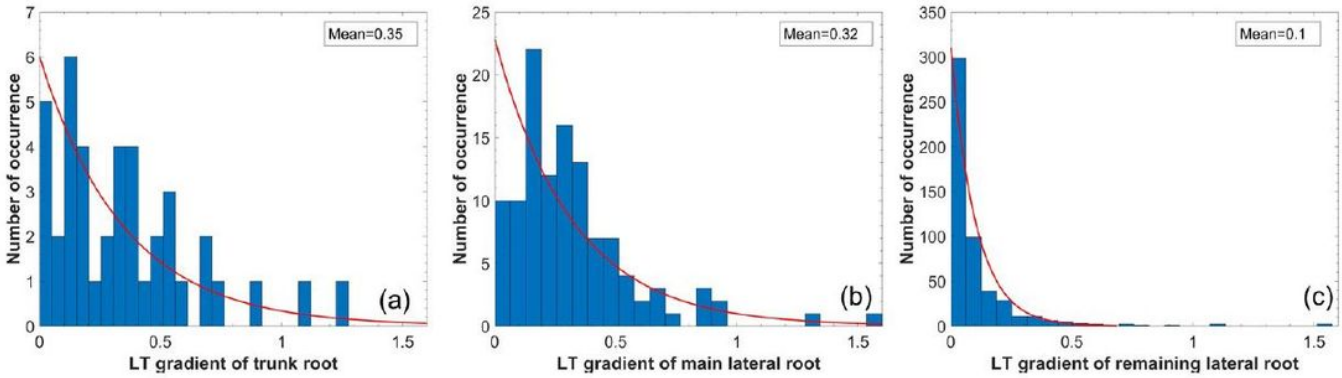

Figure 13

Histograms of the local thickness gradients (ÑLT): (a) trunk roots, (b) main lateral roots, and (c) remaining lateral roots. The mean value is determined using the exponential distribution.